A KU-BAND ATI SAR MISSION FOR TOTAL OCEAN SURFACE CURRENT VECTOR RETRIEVAL: SYSTEM CONCEPT AND PERFORMANCE

Paco López-Dekker[*], *Francesco De Zan*[*], *Steffen Wollstadt*[*], *Marwan Younis*[*],
Richard E. Danielson[†], *Volker Tesmer*[‡], *and Luis Martins Camelo* [§]
[*]German Aerospace Center (DLR), Microwaves and Radar Institute
Oberpfaffenhofen, Germany
Email: Francisco.LopezDekker@dlr.de
[†]Nansen Environmental and Remote Sensing Center (NERSC), Norway
[‡]OHB System AG, Bremen, Germany
[§]MacDonald, Dettwiler and Associates (MDA), Canada

I. INTRODUCTION

Direct measurement of ocean currents at sub-mesoscale resolutions is one of the main observational gaps left in the quest to understand the dynamics of ocean processes and ocean-atmosphere interactions. Working towards closing this gap, ESA has initiated a number of studies in order to develop a mission concept, based on a dual-beam along-track Synthetic Aperture Radar interferometer (ATI SAR) [1], [2]. One of the visible outcomes of these efforts has been the development of the Wavemill concept [3].

The basic principle behind ATI is generating a pair of SAR images of a surface under nearly identical geometry and with a short time-lag, such that the phase differences observed provide an estimate of the first moment of the Doppler spectrum associated to the surface motion. It is worth pointing out, however, that the retrieved mean Doppler frequency cannot be directly translated into an ocean current component: it provides a Normalized Radar Cross Section (NRCS) weighted average of the radial velocities, where the coupling between NRCS and velocity modulations by the underlying wave-field result in strong sea-state dependent biases. This is clearly illustrated by, for example, the strong correlation between Doppler centroid anomalies and surface winds in ENVISAT's ASAR observations [4]. In fact, the estimated Doppler shift is commonly used to help in the estimation of surface winds.

Assuming that these geophysical biases can be dealt with, for example by simultaneously resolving the surface wind vector, it is intuitively clear that ATI-SAR observations of the ocean surface can provide valuable information regarding the ocean surface current [5].

In a typical ATI configuration, with a common transmitter and two receive-phase centers separated along-track by a physical distance B_{AT}, the ATI phase ($\Delta\phi_{\mathrm{ATI}}$) is related to the effective (NRCS weighted average) radial velocity (v_r) by:

$$\Delta\phi_{\mathrm{ATI}} = -2\pi\frac{B_{\mathrm{AT}}}{\lambda}\cdot\frac{v_r}{v_{\mathrm{orb}}}, \tag{1}$$

where λ is the radar wavelength, v_{orb} the platform velocity, and where

$$\tau_{\mathrm{ATI}} = \frac{B_{\mathrm{AT}}}{2\cdot v_{\mathrm{orb}}}, \tag{2}$$

can be identified as the temporal lag between the interferometric pair. From (1) it is clear that larger baselines (expressed in wavelengths) lead to better sensitivities.

Generally speaking, during the time interval τ_{AT} the ocean surface evolves, resulting in a loss of coherence, which introduces phase estimation errors. This would limit the performance for very large baselines, so that it is intuitively clear that there is an (sea state dependent) optimal baseline. In the context of the system concept discussed in this paper, however, the physically feasible baselines are much smaller than the optimum.

Ignoring geophysical biases, ATI measurements are usually limited to measuring one component (at best) of the surface velocity vector. To overcome this limitation Frasier and Camps [2] proposed a Dual Beam Interferometer (DBI) concept, where two interferometric pairs are formed with fore and aft squinted beams.

Spatial Coverage	Global
Temporal sampling	$< 20\,\mathrm{d}$
TSCV accuracy	$5\,\mathrm{cm\,s^{-1}}$
OSWV accuracy	$2\,\mathrm{m\,s^{-1}}$
Minimum surface wind (U_{10})	$2\,\mathrm{m\,s^{-1}}$
Product resolution	$1\,\mathrm{km}$ to $4\,\mathrm{km}$
Operating frequency	Ku Band

Table I. Driving mission requirements

II. MISSION OVERVIEW

II-A. Mission requirements

The goal of the mission concept being studied is the direct measurement of the Total Surface Current Vector (TSCV) by means of along-track interferometry, in order to observe dynamic processes that do not fall under the geostrophic regime. In addition, the Ocean Surface Wind Vector (OSWV) needs to be simultaneously retrieved, as, aside of its own scientific relevance, it is required for a successful inversion of the TSCV out of the ATI data. Table I provides a summary of the driving mission requirements specified by ESA.

The mission requirements are challenging in terms of coverage (global coverage in less than 20 days) and measurement accuracy. In terms of product resolution, and from an instrument point of view, the requirements are moderate. In fact, they are so relaxed that the need to go for a SAR system may be questioned. Higher resolution intermediate products are nevertheless required in order to extract information about the wavespectra (in particular long wave swell components), and to allow higher resolution products in complex regions such as coastal areas. The requirement of operating at Ku-band is mainly driven by technological considerations (technological maturity), and may be reconsidered in the future.

II-B. Observation Concept

The proposed general instrument concept presents some commonalities but also some clear differences with respect to the Wavemill instrument concept [3], which we think are worth emphasizing. The measurement concept is to implement a dual beam-interferometer, using a single side-looking SAR system. The minimum swath width required to meet the mission objectives is roughly $150\,\mathrm{km}$, although the current goal is to provide a $200\,\mathrm{km}$ continuous swath operating in a ScanSAR mode. With respect to the two left and right looking swathes proposed for Wavemill, the single side option allows capturing larger ocean features, while simplifying the spacecraft design.

In our scientific understanding of mission, we consider an accurate inversion of winds and total current vectors out of the radar data at the required resolutions one of the main challenges. It is been shown in the literature that both the NRCS and the observed Doppler velocities are polarization dependent, as they expose the presence of different scattering mechanisms. Even in the absence of well established inversion models that exploit this sensitivity, we believe that polarization diversity will be essential to provide the required product quality. Under normal sea state conditions, the cross-polarized backscattering is much smaller than the co-polarized. With this consideration in mind, we propose a hybrid-polarimetry solution [6], using a circular polarization on transmit, in order to retrieve the vertical and horizontally polarized backscattering signals.

Another departure from the original Wavemill concept is that we propose to go to larger incident angles. This has two reasons:

i. At larger incident angles the geometrical sensitivity to horizontal velocities increases, which scales down the impact of several systematic errors.

ii. Scatterometry based wind retrieval performs better for larger incident angles.

Of course, the cost of using shallower incident angles is a significant reduction of the NRCS of the ocean surface, which translates to more demanding sensitivity requirements.

II-C. Observation Geometry

The basic geometry is that of a single-side looking javelin system concept with an electronically steered phased-array antenna. The given requirements are a swath width of $200\,\mathrm{km}$ and a squint angle on-ground close to $\pm 45°$, since this would yield a constant two-dimensional (2D) measurement sensitivity of the surface velocity. For the performance across the swath (spanned by several ScanSAR sub-swaths), one has to consider the strong variation of the squint angle on-ground as well as of the incident angle. This becomes clear when looking at an antenna pattern of any *phased array antenna* with a fixed steering angle in azimuth (projected on-ground). A ground-projected pattern is illustrated in Figure 1c, where we

can recognize that the footprint follow, as a matter of fact, an iso-Doppler line. It is also clear that this result in a range dependent ground-projected squint angle, which implies that the ideal $45°$ is only achieved at a single point.

The variation of the squint angle and also the incident angle in Figure 1a is given for an orbit height of around $800\,\mathrm{km}$ and an antenna steering angle of around $18°$.

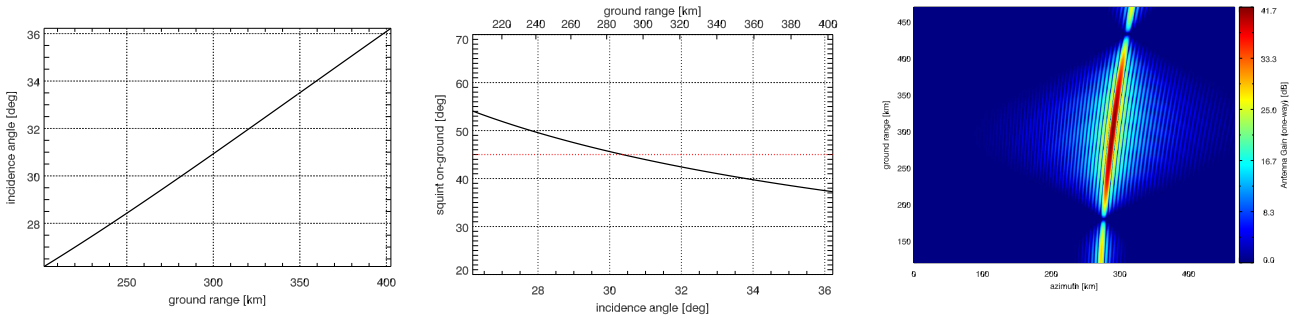

(a) (b) (c)

Fig. 1. (a) incident angle range in line-of-sight across full $200\,\mathrm{km}$ coverage, (b) Squint angle on-ground across full $200\,\mathrm{km}$ coverage, (c) Phased-array antenna pattern projected on ground covering approximately $100\,\mathrm{km}$ swath width; $18.5°$ electronically steered in azimuth; antenna size $\sim 4\,\mathrm{m}$ x $0.2\,\mathrm{m}$.

Apart from the antenna and the instrument, the final performance depends strongly on the adopted acquisition geometry. Therefore the possible geometry options for the optimization process are determined by

a) the orbit height,
b) the incident angle range (far/near range),
c) and the swath width and squint angle,

where *c*) is basically given by the requirement of $200\,\mathrm{km}$ swath width and $45°$ squint angle on-ground. Therefore *a*) and *b*) are the variables which can be modified in order to obtain a feasible system.

III. DERIVATION OF INSTRUMENT REQUIREMENTS

The instrument design has been split in two steps: first, we have derived instrument requirements from the basic interferometric performance model; subsequently, we have designed and tuned instrument architectures to meet the instrument requirements.

III-A. Performance Model

The standard deviation of the total surface current velocity is used as a direct indicator of the TSCV accuracy. This assumes the existence of an inversion algorithm capable of separating the wind-induced from the surface current components of the observed Doppler velocities. The surface velocity (radial velocity projected on-ground) can be written as

$$v = \frac{\frac{\lambda}{4\pi}\phi_{\mathrm{ATI}}}{\tau_{\mathrm{ATI}}} \cdot \frac{1}{\sin(\theta_{\mathrm{i}})}, \tag{3}$$

where θ_{i} is the incident angle.

Now we use the Cramer-Rao bound for the phase standard deviation, which is [7]

$$\sigma_{\phi_{\mathrm{ATI}}} = \sqrt{\frac{1-\gamma^2}{2N\gamma^2}}, \tag{4}$$

where γ is the coherence and N the number of independent samples.

Therefore the performance along Line-of-Sight (LoS), i.e. the standard deviation of the surface current, can be modelled as

$$\sigma_v = \frac{1}{\sin(\theta_{\mathrm{i}})}\frac{\lambda}{4\pi}\sqrt{\frac{1-\gamma^2}{2N\gamma^2}}\frac{1}{\tau_{\mathrm{ATI}}}. \tag{5}$$

Note, that the total error or accuracy of the TSCV measurement is composed of several biases and/or systematic errors. In principle there are several system biases, like e.g. baseline errors due to thermoelastic deformations, and geophysical biases, like Doppler distortions due to different ocean surface motions. The interferometric error has to be considered within this total error budget.

III-B. Methodology

Evaluation of the interferometric performance: The interferometric performance is basically the evaluation of (5) for each LoS (forward and backward looking beam) and the combination of the results in order to obtain a 2D error vector. All necessary input variables and evaluation steps are described in the following paragraphs. Basic inputs, which are not discussed in detail here, are the geometry including the various angles, the antenna pattern (cf. section II-C) and the Noise-Equivalent-Sigma Zero (NESZ) of the instrument.

Another important input is the NRCS of the surface in order to calculate the Sigma-to-Noise-Ratio (SNR) coherence γ_{SNR}. These values are calculated using the NSCAT-3 GMF (geophysical model function) of the KNMI (Royal Netherlands Meteorological Institute). NRCS values depending on a given wind speed, wind direction and incident angle are available. The NRCS ranges from $-12\,\mathrm{dB}$ to $-4\,\mathrm{dB}$ for a very low wind speed of $2\,\mathrm{m\,s^{-1}}$, but is larger for higher wind speeds (up to $3\,\mathrm{dB}$ @ $10\,\mathrm{m\,s^{-1}}$). Note that finally we end up with 2 x 2 NRCS vectors, two for the forward and backward looking beams for both horizontal (H) and vertical (V) polarizations.

Polarization reconstruction from compact-pol data and NESZ scaling: Each of the two look directions of the instrument needs an antenna configuration with two channels for transmit and receive (the detailed instrument and antenna configuration is described later in section IV). Nominally these two channels correspond to horizontal and vertical polarization. However, because of the considered phased-array antenna approach with an electrically squinted geometry, the two channels do not correspond to H or V polarizations at the surface, having defined V as the polarization with the electrical field transverse to the incident plane and H as the polarization parallel to the incident plane. This necessitates a reconstruction of the true polarizations on-ground, which is possible under the assumption that the cross-polarization is zero. The relation of channel and target polarization is depicted in Figure 2 in terms of scaling factors depending on the incident angle. These factors can be considered by scaling the noise or the NESZ, respectively. The resulting NESZ corresponds finally to the polarization at the targets and can be used for the evaluation of the SNR or γ_{SNR}, respectively. The use of circular polarized hybrid-polarization ensures that the surface is illuminated with the similar power density levels at H and V polarizations.

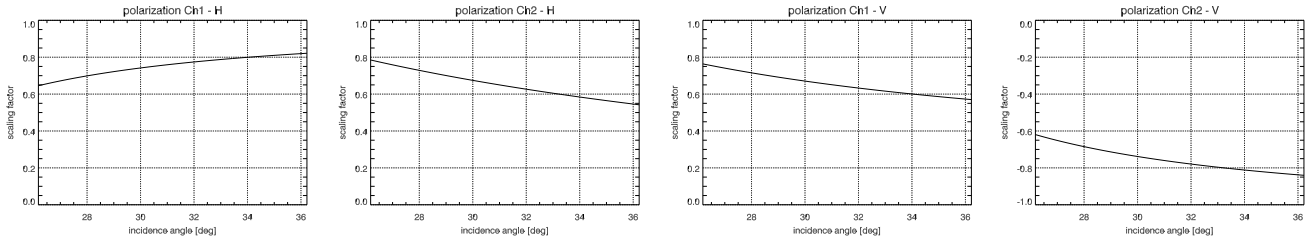

Fig. 2. Noise scaling factors (range position dependend) due to squinted geometry using a phased-array antenna: Describing the relation between instrument channel and target area polarization.

SNR and Coherence: The SNR has to be derived in order to estimate the coherence loss due to noise. After retrieving the four ocean NRCS vectors for the forward and backward looking beams in horizonal and vertical polarization from the NSCAT-3 model and reconstructing the NESZ for both target polarizations, four SNR contributions can be calculated by

$$\mathrm{SNR}_{\mathrm{lookDir,pol}} = \sigma^0_{\mathrm{lookDir,pol}} - \mathrm{NESZ}_{\mathrm{pol}} \tag{6}$$

where σ^0 represents the NRCS, $\mathrm{lookDir}$ the forward or backward look direction and pol the polarization (H or V). In total this results in four contributions, which can be translated into the coherence contribution by $\gamma_{\mathrm{SNR}} = 1/(1+\mathrm{SNR}^{-1})$, for each look direction or polarization, respectively.

Total coherence and ambiguities: Finally the total coherence, necessary in (5), can be calculated with the partial coherence multiplication rule. Additionally to the SNR coherence γ_{SNR} the following contributions are considered: The temporal decorrelation $\gamma_{\mathrm{temp}} = \exp\left(-\tau^2_{\mathrm{ATI}}/\tau_c^2\right)$, where τ_c is the coherence time [2].

A quantization decorrelation γ_{quant} is considered with a 4-bit quantization to be close to one. A 3-bit quantization coherence is assumed to be too low. The fourth and last considered contribution is the one resulting from ambiguities γ_{amb}, which can be calculated from the Distributed Target Ambiguity Ratio (DTAR) by $\gamma_{\mathrm{amb}} = 1/(1+\mathrm{DTAR})$, or vice versa.

This factor is chosen to be set to a quite high value (e.g. 0.96) in order to achieve a good ambiguity performance. In principle the decorrelation due to ambiguities is an important figure in the coherence trading-space. If no dedicated trade-off is investigated, at least one has to ensure that $\gamma_{\mathrm{amb}} \geq \gamma_{\mathrm{SNR}}$.

Number of independent samples: The number of independent samples or number of looks, respectively, is the trading factor against the NESZ. This number is in turn dependent on the final product resolution ρ_{L2} and the 2D resolution

$$\rho_{\mathrm{2D}} = \rho_{\mathrm{rg}} \cdot \rho_{\mathrm{az}} \cdot \frac{1}{\cos(\theta_{\mathrm{squint}})} = \frac{c_0}{2B_{\mathrm{rg}} \sin(\theta_{\mathrm{i}})} \cdot \frac{L}{2} \cdot \frac{1}{\cos(\theta_{\mathrm{squint}})}, \tag{7}$$

where ρ_{rg} is the slant range, ρ_{az} the azimuth resolution, L the antenna length, c_0 the velocity of light, B_{rg} the pulse bandwidth, and θ_{squint} the squint angle on-ground. Being dependent on incident and squint angle causes the number of looks $N_l = \rho_{\mathrm{L2}}/\rho_{\mathrm{2D}}$ to be varying across the swath. Fixing the bandwidth exemplarily to $10\,\mathrm{MHz}$ and the antenna length to $4\,\mathrm{m}$ results in the available number of looks shown in Figure 3a. Figure 3b shows the corresponding 2D resolution. Both figures consider a theoretical single swath case, i.e., not a burst imaging mode, and a product resolution of $4\,\mathrm{km}$ x $4\,\mathrm{km}$. Additionally we can note, that the 2D resolution vs. the NESZ is the main trade-space for designing the instrument and the pulse bandwidth plays also a major role within the instrument trading-spaces.

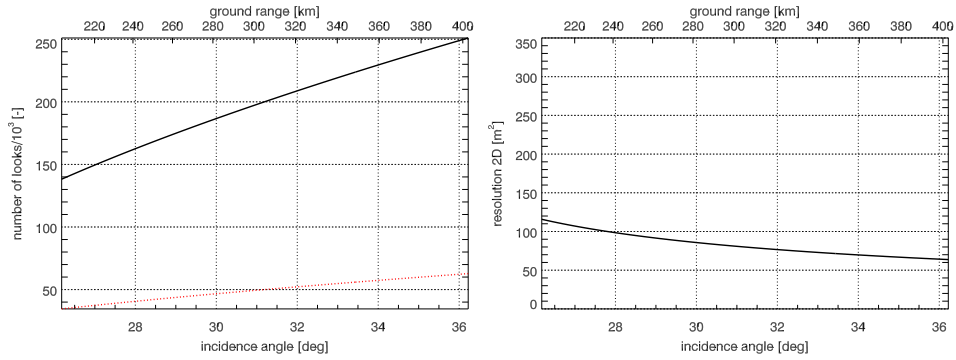

(a) (b)

Fig. 3. (a) Available number of looks for a product resolution of $4\,\mathrm{km}$ x $4\,\mathrm{km}$ (black/solid line) and $2\,\mathrm{km}$ x $2\,\mathrm{km}$ (red/dashed line), (b) Corresponding 2D resolution according to $10\,\mathrm{MHz}$ pulse bandwidth and 4 m antenna length (burst imaging mode not considered).

2D vector reconstruction: Finally all variables of (5) are available and the TSCV performance can be evaluated for each look direction (forward and backward) and polarization (H and V) separately. The last step is the combination or reconstruction of the 2D velocity vector for each point along ground range, since the four contributions are still in LoS direction, which is varying on-ground along the swath. Basically this means a geometric transformation of all back- and forward LoS error vectors into a common coordinate system, which could be azimuth and range. Finally with these two contributions a total error vector can be derived or a worst case error direction can be detected. The current speed error can be approximated by projecting the error in the direction of the current.

NESZ requirement for instrument: The interferometric performance has to satisfy the science requirements, expressed in terms of TSCV accuracy. In order to avoid an end-to-end simulation for all instrument possibilities also considering all trade-spaces, the science requirements can be traced back to typical SAR performance requirements, like NESZ and resolution.

The approach is to generate a mapping of SAR performance to TSCV accuracy using the model discussed, and use this mapping to find the trade-off space that satisfies the scientific goals. After optimizing and fixing the acquisition geometry and the along track baseline, and making some assumptions w.r.t. the effect of ambiguities and quantization levels, we can map 2D resolution and NESZ to TSCV accuracy for our threshold wind for each ground-range position. Once this is done, it is straightforward to determine, for example, the minimum required NESZ as a function of 2D resolution and ground-range position, providing the instrument designer with an explicit trade-off space.

III-C. Derived requirements

Evaluating the geometrical options given in section II-C, the favored option is a high orbit and far range, which is presented in this section. Note that this choice is non-trivial: for a given system, higher orbits result in a worse sensitivity (higher

NESZ); at the same time, with higher orbits the range of incident angles is reduced, which is favorable given the steep decline of the NRCS with increasing incident angles. The main parameters w.r.t. the instrument requirement derivation are the orbit height, the azimuth squint angle, the total swath width (cf. Table II), the incident angle range of $26°$ to $36.5°$ and the product resolution of $4\,\mathrm{km}$ x $4\,\mathrm{km}$.

Figure 4a shows the TSCV performance in m/s depending on NESZ and elevation, i.e., the standard deviation of the TSCV. Figure 4b is an extracted contour line of the requirement which gives the upper NESZ limit so that the TSCV requirement of $3\,\mathrm{cm\,s^{-1}}$ is fulfilled. The quantization result from the stepwise variation of the input. Both figures depend on a fixed resolution w.r.t. a pulse bandwidth ($10\,\mathrm{MHz}$) and an antenna length ($4\,\mathrm{m}$). The corresponding 2D resolution variation is depicted in Figure 3b and is between $63\,\mathrm{m^2}$ and $116\,\mathrm{m^2}$. The corresponding variation of incident angle and squint angle on-ground is illustrated in Figure 1b and Figure 1b.

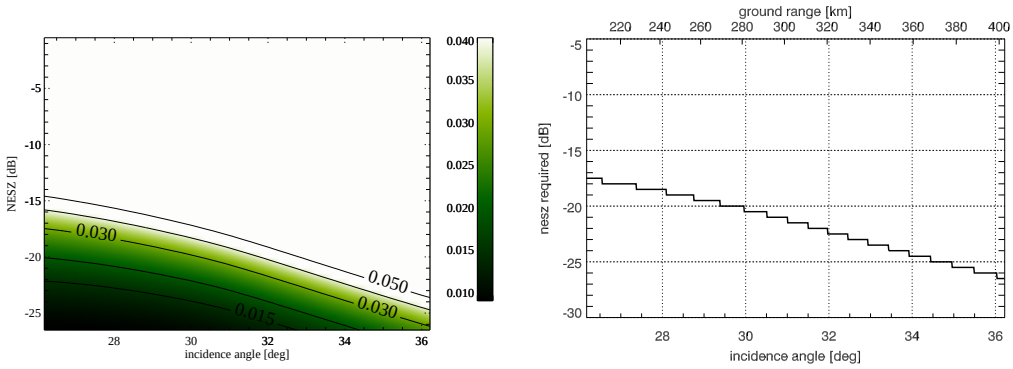

(a) (b)

Fig. 4. (a) TSCV performance in $\mathrm{m\,s^{-1}}$, (b) NESZ requirement for a TSCV error of $3\,\mathrm{cm\,s^{-1}}$.

Finally the result of the NESZ requirement for a 2D resolution range is presented in Figure 5. This allows the freedom of NESZ/resolution trading (and also azimuth vs. range resolution) within the instrument design, as well as applying e.g. different resolutions for each swath when using a burst imaging mode. One can clearly observe, that the requirement becomes stronger for coarser resolutions and towards far range.

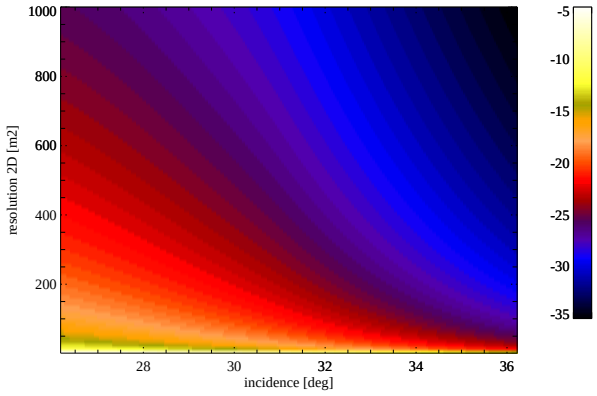

Fig. 5. NESZ instrument requirement space (in [dB]) depending on range position and 2D resolution.

IV. INSTRUMENT CONCEPT AND PERFORMANCE

The instrument requirements are demanding, in particular due to the wide-swath requirement. To achieve the performance using realistic levels of average RF power, the use of Digital Beam Forming (DBF) techniques, and in particular of the SCan-On-REcieve (SCORE) techniques, are indispensable. Given that two sets of receive antennas are needed to form the along-track interferometers, and in order to minimize losses, a canonical SCORE system is proposed. The narrow transmit

Orbit height	780 km	ATI baseline	12 m
Azimuth squint	±18.5°	Mechanical antenna tilt	20.1°
Transmit Antenna		Receive Antenna	
Length	3.6 m		3.6 m
Height	0.22 m		0.8 m
Number of rows	13		48
Directivity	43 dBi		48.6 dBi
Average transmit RF power	3 kW	Noise Temperature	400 K
Losses	2.75 dB		1 dB
Polarization	Circular		Two orthogonal channels
Operating Mode			
SAR mode	ScanSAR	DBF mode	SCORE
Number of bursts	3	Total swath coverage	210 km
Pulse bandwidth	10 MHz, 10 MHz and 10 MHz		
PRF	3.780 kHz, 3.830 kHz and 3.880 kHz		
Processed Doppler bandwidth	168 Hz, 346 Hz and 840 Hz		

Table II. Main instrument design and operating mode parameters

antennas (in elevation) are center mounted (see left panel in Figure 6), while the wider receive antennas are mounted at the ends of a deployable structure that provides the required ATI baseline.

Table II lists the main instrument and operating parameters. In the existing preliminary hardware design, losses on receive are minimized connecting a LNA for each receive element, while the desired transmit power is generated using also one medium power TWTA per row. In the baseline concept, separate physical antennas are used to generate each of the two fore and aft squinted beams, and two orthogonal linear polarizations.

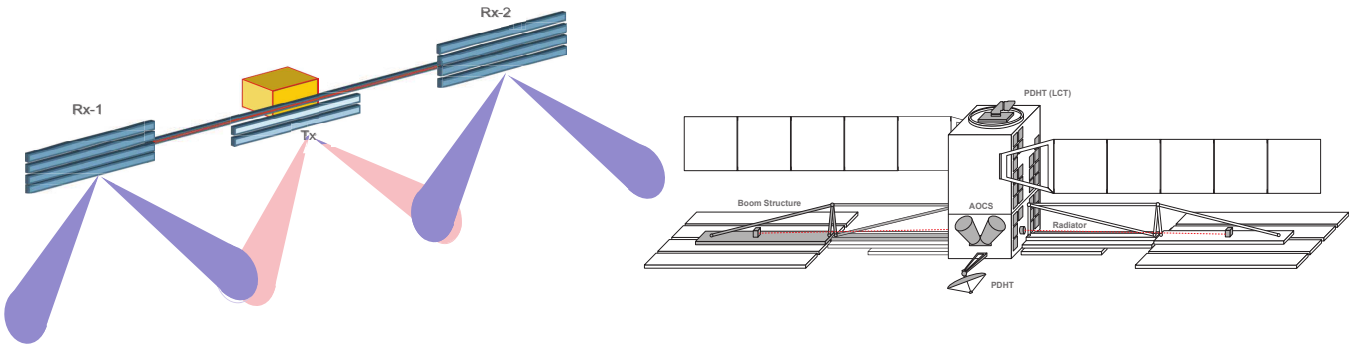

Fig. 6. Left: Instrument concept. Right: possible satellite implementation

The left panel in Figure 7 shows the single-look 2D resolution as a function of ground range (bottom axis) and incident angle (top axis) achieved by the system. For the three ScanSAR sub-swaths, the burst length and the pulse bandwidth have been optimized in order to meet the performance requirements. In particular, by improving the resolution for increasing incident angles, the NESZ requirements are partially equalized.

The right panels shows the achieved NESZ as a function of the position in the swath. For each sub-swath three relative azimuth positions are shown, revealing the scalloping associated to ScanSAR. The olive-green lines show the target NESZ for the resolution provided.

V. OUTLOOK

In this paper we have provided an overview of the mission requirements, design logic, and preliminary instrument design and performance analysis for a future Ocean Surface Currents Mission. The design derived is feasible, although the resulting spacecraft would be a relatively large Sentinel-1 class satellite. We have hinted in the paper at the major challenges associated to the inversion of the desired surface currents from the obtained data. There is a clear need for experimental research to solve (if possible) the inversion puzzle.

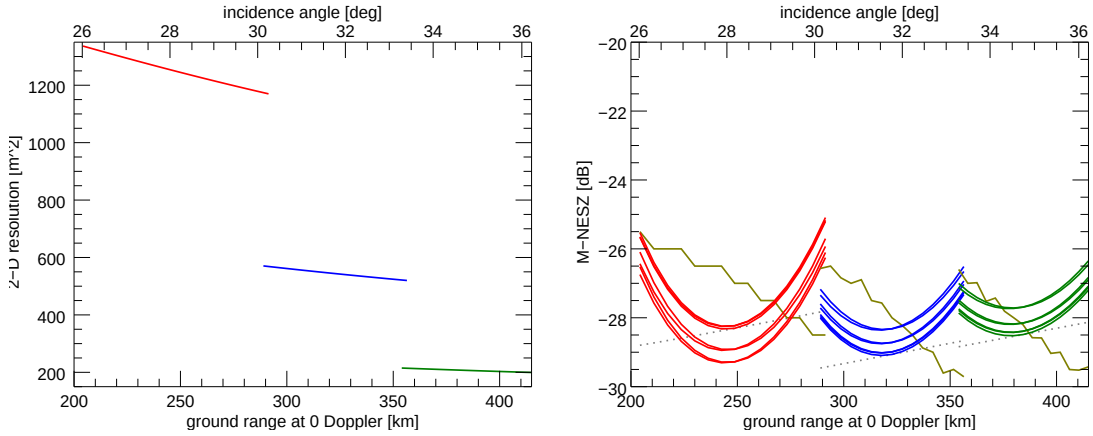

(a) (b)

Fig. 7. (a) 2D single-look resolution for proposed design, (b) Achieved NESZ.

Another major issue not discussed in this paper is the contribution of systematic errors to the overall error budget. For example, in order to achieve the overall desired $5\,\mathrm{cm\,s^{-1}}$ TSCV accuracy, the orientation of the baseline needs to be known with an accuracy better than $1\,\mu\mathrm{rad}$. Achieving this kind of baseline knowledge will require a combination of metrology with innovative calibration approaches.

VI. ACKNOWLEDGEMENT

This work has been funded by ESA-ESTEC under contract no. 4000109908/14/NL/BJ.

VII. REFERENCES

[1] R. M. Goldstein, H. A. Zebker, and T. P. Barnett, "Remote sensing of ocean currents," *Science*, vol. 246, no. 4935, pp. 1282–1285, Dec. 1989. [Online]. Available: http://www.sciencemag.org/content/246/4935/1282

[2] S. Frasier and A. Camps, "Dual-beam interferometry for ocean surface current vector mapping," *Geoscience and Remote Sensing, IEEE Transactions on*, vol. 39, no. 2, pp. 401–414, 2001.

[3] C. Buck, M. Aguirre, C. Donlon, D. Petrolati, and S. D'Addio, "Steps towards the preparation of a wavemill mission," in *Geoscience and Remote Sensing Symposium (IGARSS), 2011 IEEE International*, Jul. 2011, pp. 3959–3962.

[4] B. Chapron, F. Collard, and F. Ardhuin, "Direct measurements of ocean surface velocity from space: Interpretation and validation," *Journal of Geophysical Research: Oceans*, vol. 110, no. C7, pp. n/a–n/a, 2005. [Online]. Available: http://onlinelibrary.wiley.com/doi/10.1029/2004JC002809/abstract

[5] R. Romeiser, H. Breit, M. Eineder, and H. Runge, "Demonstration of current measurements from space by along-track SAR interferometry with SRTM data," in *Geoscience and Remote Sensing Symposium, 2002. IGARSS '02. 2002 IEEE International*, vol. 1, 2002, pp. 158–160 vol.1.

[6] R. Raney, "Hybrid-polarity SAR architecture," *IEEE Transactions on Geoscience and Remote Sensing*, vol. 45, no. 11, pp. 3397–3404, Nov. 2007.

[7] M. Seymour and I. Cumming, "Maximum likelihood estimation for SAR interferometry," in *Geoscience and Remote Sensing Symposium, 1994. IGARSS '94. Surface and Atmospheric Remote Sensing: Technologies, Data Analysis and Interpretation., International*, vol. 4, Aug. 1994, pp. 2272–2275 vol.4.